Annu. Rev. Phys. Chem. 2000. 51:209–42

EFFECTIVE INTERACTIONS BETWEEN ELECTRIC DOUBLE LAYERS

Jean-Pierre Hansen
Department of Chemistry, Cambridge University, Cambridge CB2 1EW, United Kingdom; e-mail: jph32@cus.cam.ac.uk

Hartmut Löwen
Institut für Theoretische Physik II, Heinrich-Heine-Universität, D-40225 Düsseldorf, Germany; e-mail: hlowen@thphy.uni-duesseldorf.de

Key Words density functional, charged colloids, correlations, Poisson-Boltzmann theory, Debye screening

■ **Abstract** This review summarizes and assesses recent theoretical and experimental advances, with special emphasis on the effective interaction between charge-stabilized colloids, in the bulk or in confined geometries, and on the ambiguities of defining an effective charge of the colloidal particles. Some consideration is given to the often neglected discrete solvent effects.

INTRODUCTION

Electric double layers form spontaneously whenever surfaces carrying ionizable groups are suspended in a polar solvent, most frequently water. The high dielectric constant ϵ of the latter favors the dissociation of the functional surface groups, so that the surface acquires a net charge per unit area, σ. Oppositely charged counterions are released into the solvent, which generally also contains a finite concentration of microscopic anions and cations (microions), thus providing additional coions and counterions. The electric double layer results from the buildup of a charge density (or "cloud") of opposite sign to that of the surface charge, which tends to screen the electrostatic potential due to the latter. The width of the double layer, which is a measure of its capacity, is determined by the competition between the thermal motion of the microions, which tends to spread out, or homogenize, their distribution in order to increase their entropy, and the electrostatic interactions, which attract the counterions toward the surface while repelling the coions.

This review deals with electric double layers around mesoscopic charged particles, which are referred to as polyions (frequently also called macroions), and more specifically with the effective interactions between electric double layers

associated with different polyions. Such double layers are ubiquitous in many physical, geophysical, chemical, and biological systems, including complex fluids, clay soils, polyelectrolytes (e.g. DNA), and cell membranes. The main focus of the review is on colloidal dispersions of spherical, rodlike, or lamellar polyions, or micelles resulting from the self-assembly of ionic surfactants (1). Advanced experimental techniques, such as surface force machines or video microscopy in combination with optical tweezers, allow a direct measurement of the forces acting between charged surfaces or polyions. Such direct measurements contrast with indirect determinations of effective forces via small-angle X-ray or neutron scattering measurements of static structure factors (2). For the theoretician, the main challenge is the highly asymmetric nature of dispersions involving mesoscopic polyions, and microscopic solvent molecules and ions. Clearly, at least three widely different length scales are involved, namely the characteristic size (radius) a of the polyions, a typical width of the electric double layer, on the order of the Debye screening length λ_D, and a typical correlation length l of the solvent, on the order of a few molecular diameters. Under most physical conditions, the double inequality $a \gg \lambda_D \gg l$ holds, so that a coarse-grained statistical description of the suspension is clearly warranted. This strategy may be cast in the unifying framework of the density functional theory (DFT) of inhomogeneous fluids (3), as explained in the following section. A number of key issues, which are currently the object of intense experimental and theoretical scrutiny, are addressed in subsequent sections of this review. They include the following questions and topics: (*a*) the limitations of the standard Poisson-Boltzmann or mean-field theory of electric double layers and the importance of spatial correlations between microions (a particularly important question relates to the possibility of an attractive component of the effective interaction between polyions, induced by microion correlations); (*b*) the notion of effective polyion charge (or charge renormalization), as controlled by dissociation equilibria and counterion adsorption (or condensation), and of charge regulation; (*c*) the relation between effective interactions between polyions, and the phase behavior of their dispersions; (*d*) the effect of confinement on the effective interactions between colloids, and more generally the influence of electrostatic boundary conditions at interfaces; and (*e*) the introduction of solvent granularity into the statistical description of double-layers. This review emphasizes the more recent experimental and theoretical developments in this very active field, mostly covering work published during the past decade. Earlier work is adequately covered in some previous reviews of the subject (4–7). Electrostatic CGS units are used throughout.

MULTICOMPONENT VERSUS EFFECTIVE ONE-COMPONENT DESCRIPTION

Consider a suspension of N polyions, of radius a and charge Z, in a polar solvent with co- and counterions, of radii $a_\pm$ and charges $z_\pm e$; the radius of the solvent molecules is comparable to the microion radii $a_\pm$, i.e. on the order of 0.1–0.2

nm. In micellar solutions, 1 nm $< a <$ 10 nm, and $10 < |Z| < 100$, whereas in most colloidal dispersions, 10 nm $< a < 10^3$ nm, and $10^2 < |Z| < 10^4$. A statistical description of the highly asymmetric multicomponent system is a considerable challenge, which requires some degree of coarse graining. In most theoretical investigations of micellar or colloidal systems, the solvent is regarded as a mere continuum, characterized by its macroscopic dielectric constant ϵ. This amounts to a "primitive model" (PM) level of description, where polyions and microions are assumed to be charged hard spheres (nonspherical polyions are considered later in this review) interacting via the Coulomb potential $\sim e^2/\epsilon r$, outside the excluded volume range of interparticle distances r. It is implicitly assumed that the mesoscopic polyions have the same macroscopic dielectric constant ϵ as the solvent, thus avoiding complications due to dielectric discontinuities (e.g. image charges).

Even within the PM, the theoretician is still faced with the polyion-microion asymmetry. In micellar solutions, where the size and charge ratios $a/a_\pm$ and $|Z|/|z_\pm|$ are roughly a factor of 10, the asymmetry may still be handled within the multicomponent PM level of description, using the theoretical techniques of the theory of classical fluids (8). In particular, the partial pair distribution functions $g_{\alpha\beta}(r)$ (where α and β are species indices) may be calculated from the usual fluid integral equations, including the hypernetted chain (HNC) (9) and mean spherical approximations (10), or their variants (11) and hybrid combinations (12, 13). Alternatively these correlation functions may be obtained from Monte Carlo (MC) or molecular dynamics (MD) simulations of the asymmetric PM. The multicomponent PM point of view is, in practice, limited to micellar systems with $|Z| < 10^2$ because integral equation closures are increasingly unreliable for asymmetric systems, and their numerical solution tends to become unstable. Similarly, simulations become more and more difficult and are currently limited to $|Z| \leq 60$ (14). The multicomponent PM description becomes untractable in the much more asymmetric colloidal range, which requires a coarse-grained description, based on effective interactions between polyions.

Important simplifications occur within the PM in a number of limiting situations. (*a*) In the limit of infinitely low concentration n (number per unit volume) of polyions, only a pair of these, within a solution of microions, need to be considered. The effective interaction between the two polyions (p) is then exactly given by the potential of mean force, $v_{pp}(r) = -k_B T \log[g_{pp}(r)]$ (15). The multicomponent problem reduces to that of an electrolyte of microions in the external field due to two fixed polyions, which leads to considerable simplifications in simulations (16) or the numerical solution of integral equations. (*b*) The problem may be further simplified by taking the limit $a \to \infty$; the initial dispersion then reduces to the much simpler system of an electrolyte confined between two parallel planes carrying a, generally uniform, surface charge σ. The classic problem of two interacting planar double layers goes back to the work of Gouy (17) and has been the object of considerable theoretical and experimental work, some of which is discussed in a subsequent section. (*c*) In the opposite limit of high concentration, each polyion is, at least temporarily, trapped in the "cage" formed by neighboring polyions. This

regime is reasonably described by a one-body model, where a single polyion is located at the center of a Wigner-Seitz cell, together with an inhomogeneous distribution of microions, such that the total charge inside the cell is zero. For practical purposes, the cell is chosen of a simple geometry reflecting the shape of the polyion (e.g. a spherically symmetric cell around a spherical polyion), and the electrostatic boundary conditions are chosen such as to mimic the average effect of the surrounding polyions (18, 19). Despite the considerable simplifications they imply, cell models allow valuable insight into concentrated dispersions, and these are discussed further on.

A unifying framework for the statistical description of interacting electric double layers, or, more generally, of inhomogeneous fluids and interfaces, is provided by DFT (3).

DFT and Effective Interactions

In view of the considerable polyion-microion asymmetry, it seems natural to combine a discrete representation of the former with a field description of the latter. Let $\{\mathrm{R}_i\}$ $(1 \leq i \leq N)$ denote the positions of the N polyions, assumed here to be spherical, and let $V_N^{\mathrm{dir}}\{\mathrm{R}_i\}$ be their direct interaction energy for a given configuration; V_N^{dir} is, to a good approximation, pairwise additive, with a pair potential $v_{\mathrm{pp}}(R)$, including a short-range excluded volume repulsion, the long-range Coulomb repulsion $Z^2e^2/\epsilon R$, and a van der Waals attraction (dispersion force), of intensity characterized by a Hamaker constant (1). The inhomogenous distributions of co- and counterions, in the "external" field of the polyions, are characterized by the local densities (or concentrations) $\rho_\alpha(\mathrm{r})(\alpha = +, -)$. The equilibrium densities satisfy the variational principle (3):

$$\left.\frac{\delta\Omega\left[\rho_+^*(\mathrm{r}),\, \rho_-^*(\mathrm{r})\right]}{\delta\rho_\alpha^*(\mathrm{r})}\right|_{\rho_\alpha^*=\rho_\alpha} = 0; \quad \alpha = +, -, \qquad 1.$$

where Ω is the grand potential functional of the trial densities, given by

$$\Omega\left[\rho_+^*, \rho_-^*\right] = F\left[\rho_+^*, \rho_-^*\right] - \sum_\alpha \int \Phi_\alpha(\mathrm{r})\rho_\alpha^*(\mathrm{r})\,\mathrm{dr}. \qquad 2.$$

In Equation 2, F denotes the intrinsic free energy functional, whereas $\Phi_\alpha(\mathrm{r}) = \mu_\alpha - \Phi_\alpha^{\mathrm{ext}}(\mathrm{r})$, with μ_α, the chemical potential of species α, and $\Phi_\alpha^{\mathrm{ext}}$, the external potential acting on ions of this species, equal to the sum of the interactions with the N polyions:

$$\Phi_\alpha^{\mathrm{ext}}(\mathrm{r}) = \sum_{i=1}^{N} v_{\mathrm{p}\alpha}(\mathrm{r} - \mathrm{R_i}). \qquad 3.$$

Note that in view of Equation 3, the equilibrium density profiles $\rho_\alpha(\mathrm{r})$, and the resulting grand potential Ω, depend parametrically on the polyion configuration. The chemical potentials μ_α are either fixed at some reservoir value (semigrand canonical ensemble) or determined a posteriori by the canonical ensemble

constraints:

$$\frac{1}{V}\int_V \rho_\alpha(\mathrm{r})\,\mathrm{d}\boldsymbol{r} = n_\alpha, \qquad 4.$$

where V is the total volume of the dispersion and n_α is the mean (macroscopic) concentration of α-ions.

Explicit calculations of the density profiles require some approximation for the generally unknown free energy functional F, which is traditionally split into ideal and excess parts, $F = F_{\mathrm{id}} + F_{\mathrm{ex}}$; F_{id} is known exactly:

$$F_{\mathrm{id}}[\rho_+, \rho_-] = k_\mathrm{B}T \sum_{\alpha=+,-}\int_V \rho_\alpha(\mathrm{r})\left[\log\left(\Lambda_\alpha^3\rho_\alpha(\mathrm{r}) - 1\right)\right]\mathrm{dr}. \qquad 5.$$

If $n_\alpha^{(0)}$ denotes the concentrations of some homogeneous reference state (i.e. in the absence of polyions), and $\rho_\alpha(\mathrm{r};\xi) = n_\alpha^{(0)} + \xi\Delta\rho_\alpha(\mathrm{r})$ $(0 \le \xi \le 1)$ denotes a continuous set of density profiles, such that $\rho_\alpha(\mathrm{r};\xi = 1)$ leads back to $\rho_\alpha(\mathrm{r})$, the equilibrium density profiles in the presence of polyions, then F_{ex} is given by the formally exact expression

$$\begin{aligned} F_{\mathrm{ex}}[\rho_+, \rho_-] = {} & F_{\mathrm{ex}}\left(n_+^{(0)}, n_-^{(0)}\right) + \sum_\alpha \mu_\alpha^{\mathrm{ex}}\int \Delta\rho_\alpha(\mathrm{r})\,\mathrm{dr} \\ & - k_\mathrm{B}T\sum_\alpha\sum_\beta\int_0^1 d\xi(\xi - 1) \\ & \times \int d\mathrm{r}\int d\mathrm{r}'\Delta\rho_\alpha(\mathrm{r})c_{\alpha\beta}[\{\rho_\alpha(\xi)\};\mathrm{r},\mathrm{r}']\,\Delta\rho_\beta(\mathrm{r}'). \qquad 6. \end{aligned}$$

μ_α^{ex} is the excess part of the chemical potential, whereas the $c_{\alpha\beta}[\{\rho_\alpha(\xi)\}]$ are the set of direct correlation functions for the inhomogeneous electrolyte with local densities $\rho_\alpha(\mathrm{r};\xi)$. For Coulombic systems, these decay asymptotically as $-v_{\alpha\beta}(r)/k_\mathrm{B}T = -z_\alpha z_\beta l_\mathrm{B}/r$ (where $l_\mathrm{B} = e^2/\epsilon k_\mathrm{B}T$ is the Bjerrum length). It proves convenient to subtract this from the $c_{\alpha\beta}$, leaving the short-ranged part $c_{\alpha\beta}^{\mathrm{sr}}$. The excess free energy function then splits into a mean-field Coulombic contribution and a correlation part:

$$\begin{aligned} F_{\mathrm{ex}}[\rho_+, \rho_-] &= F_{\mathrm{Coul}} + F_{\mathrm{corr}} \\ &= \frac{e^2}{2\epsilon}\int \mathrm{dr}\int \mathrm{dr}'\frac{\rho(\mathrm{r})\rho(\mathrm{r}')}{|\mathrm{r} - \mathrm{r}'|} + F_{\mathrm{corr}}, \qquad 7. \end{aligned}$$

where $\rho(\mathrm{r}) = z_+\rho_+(\mathrm{r}) + z_-\rho_-(\mathrm{r})$ is the microion charge density. The correlation term is formally given by Equation 6, with $c_{\alpha\beta}^{\mathrm{sr}}$ replacing $c_{\alpha\beta}$.

Starting from these exact expressions, there are basically two strategies to proceed with approximations. (*a*) The most common strategy focuses on the density profiles and the resulting free energies. F_{corr} is approximated by a local density ansatz or by some weighted density approximation (WDA) (3, 20), which generally

requires the direct correlation functions in a homogeneous reference state as input. Once the variational problem Equation 1 has been solved for the approximate free energy functional, the effective interaction energy between polyions is given by

$$V_N(\{\mathrm{R_i}\}) = V_N^{\mathrm{dir}}(\{\mathrm{R_i}\}) + \Omega(\{\mathrm{R_i}\}), \qquad 8.$$

where the equilibrium grand potential accounts for their indirect interactions, induced by the microions, which have effectively been traced out. It is important to realize that this contribution depends on the thermodynamic state of the dispersion, and is generally not pair-wise additive. If correlations are neglected altogether, F_{ex} reduces to the mean-field Coulombic part, and Equation 1 immediately leads to the equilibrium profiles

$$\rho_\alpha(\mathrm{r}) = \zeta_\alpha \exp\left\{-\left[\Phi_\alpha^{\mathrm{sr}}(\mathrm{r}) + z_\alpha e\psi(\mathrm{r})\right]/k_{\mathrm{B}}T\right\}, \qquad 9.$$

where ζ_α is the fugacity of species α (equal to its reservoir concentration in the absence of correlations), $\Phi_\alpha^{\mathrm{sr}}$ is the short-range (excluded volume) part of the interaction of an ion α with the N polyions, and $\psi(\mathrm{r})$ is the total electrostatic potential at r, which satisfies Poisson's equation:

$$\nabla^2\psi(\mathrm{r}) = -\frac{4\pi e}{\epsilon}[\rho^{\mathrm{ext}}(\mathrm{r}) + \rho(\mathrm{r})], \qquad 10.$$

with $\rho^{\mathrm{ext}}(\mathbf{r})$ the "external" charge density carried by the N polyions. Equations 9 and 10 constitute the multicenter version of mean-field nonlinear Poisson-Boltzmann (PB) theory. Despite their apparent simplicity, numerical solution of the PB equations in the presence of N polyions is a formidable task. In practice, Equation 10 is often solved in the domain outside the polyions, and the contribution of the latter to the electrostatics is treated as a boundary value problem. (*b*) A second, more ambitious strategy is to seek information on both the density profiles and the pair correlations between microions within the double layers. This may be achieved by relating the direct correlation functions, appearing in Equation 6, to their functional inverses, the total correlation functions $h_{\alpha\beta}$, via the Ornstein-Zernike relations for inhomogeneous fluids (8), supplemented by an approximate closure relation between the h and c functions. This strategy leads to coupled equations for the density profiles and the pair correlation functions, as in the widely used inhomogeneous HNC theory (21). In view of its numerical complexity, this strategy can only be applied to very simple geometries, and in practice it is limited to planar geometry.

Cell Model

As stated earlier, cell models, involving a single polyion, prove useful to study concentrated dispersions, including colloidal crystals. The paradigm is provided by the much studied case of a globular polyion of radius a, placed at the center of a spherical cavity of radius R determined by the polyion concentration, i.e. $R = (3/4\pi n)^{1/3}$, containing counterions and salt, which ensure overall charge neutrality.

The density profiles $\rho_+(r)$ and $\rho_-(r)$ depend only on the distance r from the center (one-dimensional problem). Gauss's law implies the boundary conditions that the electric field vanish on the surface of the cell, i.e. $d\psi/dr|_{r=R} = 0$. The field on the surface of the particle (i.e. at $r = a$) is determined by the surface charge density σ. Finally, because of the boundary conditions at $r = R$, the osmotic pressure P of the microions is given by (19)

$$P = k_B T[\rho_+(R) + \rho_-(R)]. \quad 11.$$

PB theory, embodied in Equations 9 and 10, reduces here to a spherically symmetric one-center problem, giving rise to a simple second-order nonlinear differential equation for the local potential $\psi(r)$, which is easily solved numerically (22, 23). Improvements over the mean-field approximation are achieved by including correlations within the local density ansatz or the weighted density approximation (23, 24). The resulting osmotic pressures are consistently lower than those predicted by PB theory, by a factor of three or more for highly charged polyions. This trend is confirmed by MC simulations of the cell model (23, 24).

Cell model calculations have been extended to other geometries, e.g. rods or platelets in cylindrical cells. They prove useful in the determination of effective polyion charges, as discussed below.

CHARGE REGULATION AND RENORMALIZATION

Most published work on electric double layers is based on the assumption of constant charge on the polyions, e.g. in the form of a uniform surface charge. This is clearly an oversimplification, as would be the other extreme assumption of constant surface potential, for two reasons: the strong coupling between electrostatics and chemical dissociation equilibrium at the surface (charge regulation), and the adsorption and strong physical binding of counterions to the surface, often referred to as counterion condensation, which leads to a reduction of the apparent polyion charge seen at larger distances (charge renormalization).

Charge Regulation

The bare (or structural) surface charge of most polyions results from the dissociation of functional groups such as the sulphate or carboxylic groups, the number of which may be measured by titration (25). Generally, the ionization is only partial, and the dissociation equilibrium, governed by a law of mass action, depends on the local ionic environment, e.g. on local salt concentration or pH. Any variation of this environment, linked to the relative motion of neighboring polyions, will lead to a fluctuation of the surface charge, but for given macroscopic conditions, one may define some average bare charge. From a theoretical point of view, the coupling of the surface chemistry to the local inhomogeneities induced by electrostatics poses a difficult challenge. Early attempts were based on a combination of the law of

mass action with PB theory (26). A more microscopic point of view is adopted in the charge regulation primitive model (27) (see also 28), which adds a strong attraction of chemical origin to the short-range part $v_{p\alpha}^{sr}$ of the polyion-microion pair potential, such that

$$\exp\left\{-v_{p\alpha}^{sr}(r)/k_BT\right\} = V_\alpha\delta(r-d_\alpha); \quad r < \frac{1}{2}(a+a_\alpha)$$

$$= 1; \quad r > \frac{1}{2}(a+a_\alpha). \qquad 12.$$

This corresponds to an infinitely deep and narrow potential well localized on a sphere of radius d_α from the center of the polyion; in practice, d_α must be chosen to be smaller than the polyion radius a, to prevent the chemical binding of the same microion to two polyions.

The pair structure of the model has been analyzed by diagrammatic expansion, and by numerical solutions of the HNC equation for small polyions corresponding to mineral oxide particles (27). The charge regulation strongly affects the effective interaction between spherical particles (discussed later).

Charge Renormalization

The bare (or structural) charge resulting from the dissociation equilibrium is frequently large, typically $|Z| \geq 10^4$ for polyion radii $a \geq 10^2$ nm. To describe electric double layers near such highly charged polyions, the traditional phenomenological approach is to divide the counterions into two populations. The first includes ions that are tightly bound (or adsorbed) to the surface by the strong electric field $E = 4\pi\sigma/\epsilon$, thus forming a so-called Stern layer of "condensed" counterions. A rough estimate of the thickness Δ of a Stern layer is obtained by balancing the electrostatic work $E \times ze \times \Delta$ against the thermal energy k_BT. The resulting $\Delta = \epsilon k_BT/4\pi\sigma ze$ is on the order of a few angstrom in water at room temperature for typical surface-charge densities and monovalent counterions; thus Δ is comparable to the size of microions, so that the "condensate" may be expected to be roughly a monolayer. This monolayer, of opposite sign to the surface charge, strongly compensates the latter, reducing the total polyion charge to an effective charge Z^* significantly smaller than the bare charge Z. The remaining counterions feel a much reduced "external" potential and form the "diffuse" part of the double layer, which can often be treated within linearized PB theory (LPB).

The phenomenological approach is to consider Z^* as a parameter adjusted to experimental data, e.g. polyion structure factors determined by light scattering (2, 29–31), but much recent theoretical effort has gone into determining the effective charge from first principles. Most schemes are based on the observation that the asymptotic behavior of the potential or density profiles is correctly described by the simple exponential screening predicted by LPB theory. Charge renormalization should account both for nonlinearities in the mean-field PB approach and for microion correlations. Early attempts focused on the single polyion problem

within the cell model (22, 23). Within LPB theory the electrostatic potential in a spherical cell is easily calculated to be of the form

$$\psi(r) = C + \frac{Ze}{\epsilon r}(Ae^{\kappa_D r} + Be^{-\kappa_D r}), \qquad 13.$$

where $\kappa_D = 1/\lambda_D$ is the inverse Debye screening length

$$\kappa_D = \left(4\pi l_B \sum_\alpha n_\alpha z_\alpha^2\right)^{1/2}. \qquad 14.$$

The integration constants A and B are determined by the boundary conditions at $r = a$ and $r = R$; C is conveniently chosen such that $\psi(r = R) = 0$. The validity of the LPB approximation is expected to be reasonable on the cell surface, but to be very poor near the polyion surface if the latter is highly charged. The bare charge Z appearing in the LPB potential Equation 13 is then adjusted to a (lower) effective value Z^* by requiring that the resulting microion charge density on the cell surface, $\rho(R)$, match the corresponding density obtained from a numerical integration of the PB equation under the same boundary conditions (22). In view of the latter, and of Poisson's equation, this means that the resulting LPB potential matches the nonlinear PB potential at the surface up to the third derivative. Note that a renormalization of Z also implies a renormalization of κ_D at a low (or vanishing) concentration of added salt. Because LPB theory underestimates the charge density near the polyion surface, it overestimates $\rho(r = R)$, compared with the PB charge profile, so that Z^* is always lower than Z. $Z^* \to Z$ for low polyion charge, then increases with Z, but saturates for high values of the bare charge, as a consequence of counterion condensation; the degree of counterion condensation is not greatly affected by salt concentration (22). The saturation value of Z^* is roughly proportional to the polyion radius a.

The effects of microion correlations on the values of Z^* have been investigated with local density ansatz and weighted density approximation versions of DFT, and by MC simulations (23, 24). Correlations tend to lead to a further decrease of Z^* compared with Z, and even to a maximum value, followed by an actual decrease of Z^* as a function of Z (23). If the effective charge is obtained by matching the LPB osmotic pressure to "exact" MC estimates, the resulting Z^* turns out to depend only weakly on the ratio a/R, i.e. on the concentration of polyions.

Other semi-phenomenological criteria for determining the effective charge are discussed by Belloni (32). The Debye-Hückel-Bjerrum theory, which has proved very successful for describing the phase behavior of PM electrolytes (33) has been extended to charged colloids (34). The Bjerrum pairs of simple electrolytes are replaced by clusters involving each a polyion and a variable number of adsorbed counterions, which are in chemical equilibrium with the free, nonadsorbed counterions, assuming a simple form for the internal partition function of a cluster. The distribution of cluster sizes turns out to be sharply peaked, allowing a clear-cut definition of Z^* (34).

A more fundamental approach to a definition of effective charges is based on a careful analysis of the asymptotic decay of density profiles and correlation functions. This may be achieved within the "dressed ion" reformulation of linear response theory, i.e. of the polarization of an electrolyte by the average electrostatic potential (35). Within the PM, the point charges of the microions are replaced by a local, spread-out charge distribution incorporating the short-range fraction of the polarization charge around each bare ion, which is thus replaced by a dressed ion. The short-range fraction of the polarization charge is defined in terms of short-range contributions $h_{\alpha\beta}^{\mathrm{sr}}$ to the pair correlation functions $h_{\alpha\beta}(r) = g_{\alpha\beta}(r) - 1$; the $h_{\alpha\beta}^{\mathrm{sr}}$ are related to the short-range parts $c_{\alpha\beta}^{\mathrm{sr}}$ of the direct correlation functions, introduced after Equation 6, via coupled Ornstein-Zernike (OZ) relations (36). This leads to an exact, nonlocal generalization of the LPB equations, and a residue analysis of the corresponding Fourier transform of the potential $\psi_i(r)$ around an ion i leads to the following asymptotic decay for large r (35, 36):

$$\psi_i(r) \sim \frac{z_i^{\ddagger} e \exp(-\kappa r)}{\epsilon^{\ddagger} r}. \qquad 15.$$

This is precisely of the LPB (or Debye-Hückel) form, but with renormalized values $z_i^{\ddagger}$, κ and $\epsilon^{\ddagger}$ of the valence, inverse screening length and dielectric constant of the solution (as opposed to the pure solvent), which can all be expressed in terms of the $h_{\alpha\beta}^{\mathrm{sr}}$; the latter may be calculated by supplementing the OZ relations with some approximate closure, e.g. HNC.

In the weak-coupling limit of very low ionic bulk concentration, $z_i^{\ddagger} \to z_i$, $\kappa \to \kappa_{\mathrm{D}}$, and $\epsilon^{\ddagger} \to \epsilon$. Simple Stillinger-Lovett sum rule (37, 37a) considerations show that proper inclusion of the finite size a_α of the ions leads to an enhancement of screening, i.e. $\kappa > \kappa_{\mathrm{D}}$ (38). For sufficiently strong coupling (i.e. at high ionic concentrations), the exponential decay Equation 15 goes over to a damped oscillatory behavior characterized by a pair of complex conjugate inverse decay lengths κ and κ^* (38–40). The location of the cross-over from monotonous to oscillatory decay depends on the approximate closure.

The dressed ion reformulation for the bulk PM may be extended to the case where one ionic species consists of polyions, and hence z_i^* is to be identified with the effective charge Z^* of the latter (36). A similar treatment has been applied to planar electric double layers to determine effective surface charge densities (41). The latter tend to saturate for monovalent counterions, increasingly so as their concentration increases, whereas for concentrated solutions of divalent ions, the effective surface charge goes through a maximum before decreasing as the bare surface charge increases. This behavior is reminiscent of that observed in a spherical cell (23, 24).

The effective polyion charge Z^* is not easily accessible to experiment. Indirect determinations are based on the assumption of the validity of some simple functional form of the effective pair interaction between polyions, generally a screened Coulomb potential. The thermodynamic properties and pair structure of a system of polyions interacting via this potential can be determined

accurately from fluid integral equations or simulations (42, 43). The effective charge Z^* is then adjusted to provide the best theoretical fit to experimental data, e.g. the polyion pair structure as measured by scattering experiments (2, 29–31), or the freezing line as a function of salt concentration and bare particle charge (44). The latter measurements confirm the saturation predicted by the PB cell model (22, 23) but should be reanalyzed because the underlying simulation data do not take into account an important "volume" contribution to the free energies, which strongly affects the phase diagram at low salt concentration (45, 46).

Recent experiments carried out at very low electrolyte concentration on silica particles, with weakly dissociating silanol surface groups, and on latex particles, with strongly dissociating sulfonic acid groups, were able to measure simultaneously the bare polyion charges by conductometric titration and the effective charges by conductivity measurements (47, 48). The bare charge was controlled by varying the amount of added NaOH. Under these experimental conditions, Z^* was not observed to saturate, but to follow very nearly a square root law $Z^* \sim \sqrt{Z}$ for both colloidal systems.

PLANAR GEOMETRY

The simplest, and most widely studied, double layer geometry is that of uniformly charged, infinite planes in an ionic solution (17). These planes may represent stacks of thin charged lamellae, such as clay platelets or rigid membranes, or they may correspond to the surfaces of spherical colloidal particles separated by a distance $h \ll a$, so that the curvature of the facing surfaces may be neglected in first approximation. In the former situation, one may consider the simplified model of a single charged plane within a slab of thickness h equal to the mean spacing between lamellae in the stack; this would be the one-dimensional equivalent of the cell model. The two situations are shown schematically in Figure 1; σ denotes the surface charge density, ϵ is the macroscopic dielectric constant of the solvent (within a PM representation), and ϵ' is the dielectric constant of the colloidal particles. When $\epsilon' \neq \epsilon$, which is the rule rather than the exception, the dielectric discontinuity at $z = \pm h/2$ must be properly incorporated into the boundary condition, e.g. by the introduction of electrostatic image charges (49). In most published theoretical work, the assumption $\epsilon' = \epsilon$ is made for the sake of simplicity.

Microion density profiles $\rho_+(z)$ and $\rho_-(z)$ depend only on z, and the intrinsic free energy functional per unit area perpendicular to the z axis is still given by Equations 5–8, with the volume integrals replaced by one-dimensional integrals over the interval $[-\frac{h}{2}, \frac{h}{2}]$. Fixed charge (or Neumann) boundary conditions imply that the potential satisfy

$$-\left.\frac{d\psi}{dz}\right|_{z=\pm\frac{h}{2}} = \pm\frac{4\pi\sigma}{\epsilon}. \qquad 16.$$

The key physical quantity, which is in principle measurable using a surface force

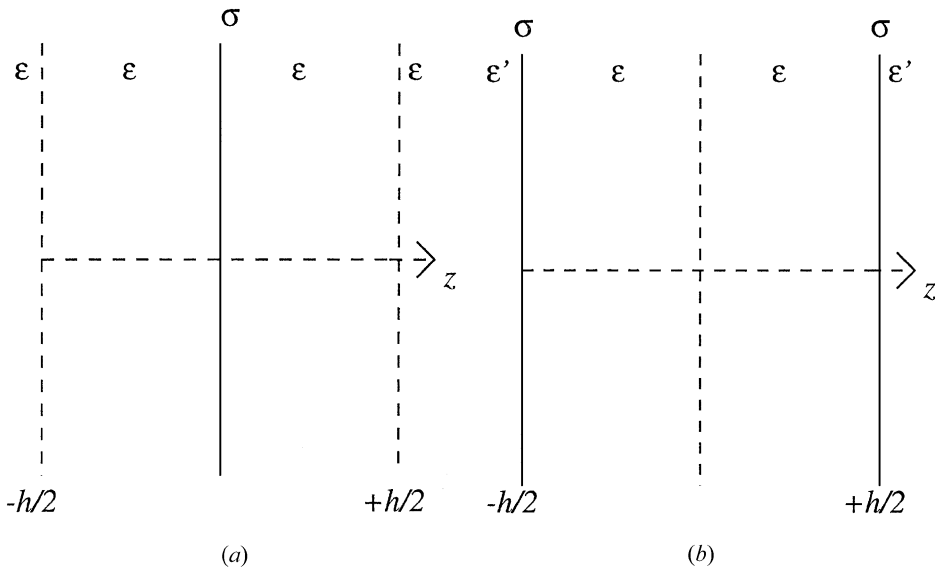

Figure 1 Two different plate geometries.

apparatus (1), is the force per unit area acting between two charged planes and their associated electric double layers. This force per unit area is the net osmotic pressure (or disjoining pressure) $\Delta P = P - P_{\text{bulk}}$, where P is the osmotic pressure exerted by the microions between the charged plates, and P_{bulk} is the pressure of the electrolyte in the reservoir that fixes the chemical potentials of the microions. P may be calculated via the mechanical route, by averaging the local stress tensor, or by the thermodynamic route, by differentiation of the total free energy, or grand potential, with respect to h. Both routes lead to a natural separation of the pressure P into kinetic, electrostatic, and collisional parts (49):

$$P = P_{\text{kin}} + P_{\text{el}} + P_{\text{coll}}, \qquad 17.$$

where

$$P_{\text{kin}} = k_{\text{B}} T \sum_{\alpha} \rho_{\alpha}(z). \qquad 18.$$

Explicit expressions for P_{el} and P_{coll} in terms of density profiles and inhomogeneous pair correlation functions are given elsewhere (49). Note that although each of the terms in Equation 17 depends on the coordinate z, their sum must be independent of z for mechanical equilibrium. In practice, simplified expressions are obtained by calculating P in midplane ($z = 0$ in Figure 1) or at the surface of the charged planes.

In the latter case, the expression for P reduces to the simple contact theorem (5):

$$P = k_B T \sum_\alpha \rho_\alpha(z = \pm(h/2 - a_\alpha)) - \frac{2\pi\sigma^2}{\epsilon}. \quad 19.$$

This expression is not convenient for simulation purposes because P appears as a difference of two large numbers, the first of which involves the contact value of the counterion density profile, affected by large numerical uncertainties. The calculation at midplane is then preferable because the ρ_α are expected to be close to their bulk values there, but the average force between microions on both sides of this plane must be evaluated (50).

Poisson-Boltzmann Approximation

The mean-field approximation, where correlations between microions are neglected, is well understood as a result of the pioneering work of Gouy (17); density profiles and forces are known analytically or are given by simple quadratures (51). The pressure is given throughout by

$$P = k_B T \sum_\alpha \rho_\alpha(z) - \frac{\epsilon}{8\pi}[E(z)]^2, \quad 20.$$

where $E(z) = -d\psi(z)/dz$ is the mean local electric field. This is most easily evaluated in the midplane, where $E = 0$ by symmetry, i.e. $P = k_B T \sum_\alpha \rho_\alpha(0)$, showing that the force between equally charged plates is always repulsive within PB theory.

In the limit of low surface charge and electrolyte concentration, PB theory may be linearized, and the disjoining pressure reduces to

$$\Delta P = 2\sigma^2 e^{-\kappa_D h}. \quad 21.$$

A charge renormalization to account for nonlinearities, similar to the procedure within the cell model described earlier, leads to a much reduced effective surface charge σ^*, and to a saturation for large bare charges σ (52).

The Effect of Microion Correlations

Although PB theory always predicts a purely repulsive interaction between planar electric double layers, it was suggested by Oosawa as early as 1968 (53) that the force might turn attractive if microion correlations were taken into account. The first convincing evidence for double-layer attraction came from MC simulations that indicated large deviations from the predictions of PB theory in the presence of divalent counterions (50). This early prediction of an attractive minimum in the effective force between planar double layers at short separations h was confirmed by subsequent simulations in the presence of salt (1:2 and 2:2 electrolytes) (49, 54) and polyvalent counterions (55), by inhomogeneous HNC calculations (49) and

an improved version based on the reference HNC closure (56, 57), and by local density ansatz and weighted density approximation versions of DFT (58, 59).

The reduction of the double-layer repulsion and eventual correlation-induced attraction may be understood by considering the contact theorem (19), or the expression for the pressure in midplane. At contact, the correlations keep the counterions in the first layer apart, thus limiting the piling up following from the uncorrelated mean-field treatment and reducing the contact value of the counterion density; according to Equation 19, this leads to a lowering of the pressure, which can even become negative (corresponding to an effective attraction), because of the negative Coulombic contribution. The lowering of the counterion concentration immediately at contact leads to an enhanced attraction of the next layers of counterions to the surface, so that correlations enhance the counterion density in that region. This enhancement in turn entails a depletion of the counterion density in the midplane, whereas electrostatic correlations make a negative contribution ($P_{\rm el}$ in Equation 17), which generally dominates the smaller, positive collisional part. Overall these various effects lead to a much reduced ΔP compared with the repulsive PB interaction. The attraction observed for very short separations may be explained by a two-dimensional, lattice-like structuring of the adsorbed counterions, when the counterion patterns on opposite surfaces are shifted relative to each other to minimize the electrostatic interactions (60).

The reason an attraction is in general observed only with divalent (e.g. Ca^{2+}) counterions is that the entropic cost associated with their "condensation" near the surface is smaller than for monovalent ions, because only half as many counterions are needed to provide the same electrostatic shielding. Another related aspect of microion correlations is the phenomenon of charge reversal (or inversion). The apparent charge density of the surface placed at $z = -h/2$, seen at the abscissa z, is (61)

$$\sigma^*(z) = \sigma + e\int_{-\frac{h}{2}}^{z} \sum_{\alpha} z_\alpha \rho_\alpha(z')\, dz'. \qquad 22.$$

Within PB theory, σ^* never changes sign, but in the presence of correlations this may occur at a critical z, beyond which σ^* is of opposite sign to σ, due to an overcompensation of the bare surface charge by the counterions. Thus a test charge will be attracted, rather than repelled, by a plane carrying a surface charge σ of the same sign, beyond a critical separation. Charge inversion can only occur when the microion density profiles have a nonmonotonic behavior. The overcompensation of the surface charges of two parallel plates is enhanced when the counterions are linked together to form polyelectrolyte chains, once more as a result of the reduction in entropic repulsion (61, 62).

Charge inversion and effective attraction between platelets may even be observed in the case of monovalent counterions, provided the coions are larger than the counterions (57).

Attractive forces between charged surfaces immersed in aqueous solutions of $CaCl_2$ and $Ca(NO_3)_2$ have been measured directly with a surface-force apparatus

(63). The existence of correlation-induced attraction between charged surfaces of equal sign has important consequences on colloid stability and provides a plausible explanation for the common observation that the addition of multivalent ions to solutions or suspensions of polyions often leads to precipitation.

SPHERICAL POLYIONS

Aqueous solutions and dispersions of spherical or quasi-spherical polyions, including globular proteins and charge-stabilized colloidal particles, such as silica mineral particles or polymer latex spheres, have been thoroughly studied experimentally and theoretically for many decades. Much of the interest stems from the realization that such colloidal systems exhibit a phase behavior reminiscent of that of simple molecular systems, albeit on very different scales. A particularly attractive feature of colloidal dispersions is that the effective interactions between particles may be tuned by the experimentalist, e.g. by varying the concentration of added electrolyte, thus providing an additional handle on phase behavior. The beautiful early microscopy observations by Hachisu et al (64) unambiguously showed the existence, at low volume fractions, of colloidal crystals and crystalline alloys, which Bragg-reflect visible light and are, in particular, responsible for the iridescence of opals.

The coexistence of ordered crystalline and disordered fluid phases has been monitored by careful experiments using confocal laser scanning microscopy, which allows the direct observations of ordered and disordered configurations, and ultra–small-angle X-ray scattering (USAXS), which provides statistically averaged information on ordering of colloids via the static structure factor $S(k)$ (47, 48). These measurements provide three-dimensional phase diagrams by varying the colloid concentration n or packing fraction $\eta = 4\pi na^3/3$, the effective colloid charge Z^* (as determined by conductivity measurements), and the monovalent salt concentration n_s, equal to the concentration n_- of coions, typically in the range 10^{-6}–10^{-5} M. The observed phase diagrams exhibit a striking reentrant behavior, e.g. for fixed n and n_s, and the colloidal dispersion crystallizes into an ordered BCC lattice on increasing Z^*, as one might expect, but on further increase of Z^*, it remelts into a disordered fluid phase. This reentrant behavior may be qualitatively understood in terms of an increase of the total ionic strength, linked to an increase of the counterion concentration n_+ with Z^*, which enhances the screening power of the microions and hence reduces the range of the screened Coulomb repulsion between polyions. However, the standard Derjaguin-Landau-Verwey-Overbeek (DLVO) representation of the latter (65) fails to provide a quantitative explanation of the experimental data (66).

Another striking feature of low concentration dispersions ($\eta < 0.05$), reported by the Kyoto School, is the appearance of strongly inhomogeneous patterns in highly deionized samples. USAXS measurements and confocal laser scanning microscopy show clear evidence of regions of relatively high colloid concentration,

which may be crystalline (67), amorphous (68), or fluid (69) in character, coexisting with regions of extremely low concentration, or voids. Apart from direct visual observation, the existence of voids, and the fraction of the total volume occupied by them, may be inferred from a comparison between the mean interparticle spacing, $d_n \sim n^{-1/3}$, calculated under the assumption of a homogeneous dispersion, and the spacing d_x deduced from the position of the main X-ray diffraction peak in the structure factor $S(k)$. The observation that d_x is significantly less than d points to the existence of voids occupying a fraction $f = 1 - (d_x/d)^3$ of the total sample volume. The considerable literature on the subject is summarized elsewhere (70). The existence of voids and the related but controversial (71) observation of a complete separation between a high concentration colloidal "liquid" phase and a much more dilute "gas" phase (72) are claimed to be evidence for a long-range attractive component of the effective pair interaction between colloidal particles carrying charges of equal sign. The same attraction is also invoked to explain the reentrant liquid-solid coexistence described earlier (66).

However, recent direct measurements of the effective interaction between pairs of colloidal particles show no evidence of an attraction, at least at low concentration. Such direct measurements are based on video microscopy. In the simplest method, a large number of instantaneous configurations of a dilute suspension are recorded, and the colloid-colloid pair distribution function $g(r)$ is calculated from the measured distribution of interparticle distances (73). The effective pair potential coincides with the potential of mean force in the low concentration limit (8) and is hence given by

$$v(r) = -k_B T \log[g(r)]. \qquad 23.$$

An alternative method follows the relative Brownian motion of a pair of colloidal particles released from initial positions where they were localized by optical tweezers (74). Both sets of measurements confirm that the effective pair potential is purely repulsive and may be fitted to a screened Coulomb (DLVO) form by adjusting the effective charge Z^* and the inverse screening length κ_D, compatible with estimated salt concentrations. However, this same DLVO potential, used within a harmonic approximation, seems to be unable to reproduce the measured bulk modulus of a colloidal crystal at much higher concentrations (75, 76), although the difference between experiment and theory may be linked to the omission of the "volume" contribution to the effective interaction energy between polyions (discussed below).

DLVO Theory Revisited

The effective pair potential between spherical polyions, first derived by Derjaguin, Landau, Verwey, and Overbeek (65), is easily recovered within the framework of DFT. On tracing out the microion degrees of freedom, the effective interaction energy between polyions is given by Equation 8, once the grand potential Ω has

been determined from the variational principle Equation 1. The required intrinsic free energy functional is defined by Equations 5 and 7. Neglecting F_{corr} in the latter amounts to mean-field theory, and the Euler-Lagrange equation associated with the variational principle leads back to the PB Equation 10 for the local electrostatic potential $\psi(\mathrm{r})$. Because the external charge associated with N polyions is a multicenter distribution, the numerical task of solving the PB equation for N interacting polyions can only be handled numerically using advanced optimization techniques, coupling MD simulations with DFT (77–79).

A more phenomenological approach may be adopted whereby the bare polyion charge is reduced to a considerably lower effective value by a Stern layer of tightly bound counterions. The coupling between the polyions and the remaining microions (forming the so-called diffuse double layer) is accordingly strongly reduced, so that the corresponding density profiles $\rho_\alpha(\mathrm{r})$ vary much more smoothly in the vicinity of the polyion surfaces. In that case, the integrands of the ideal contribution to F in Equation 5 may be expanded to second order in the deviations $\Delta\rho_\alpha(\mathbf{r}) = \rho_\alpha(\mathbf{r}) - n_\alpha$ of the local densities from their bulk values, i.e.

$$F_{\text{id}} \approx \sum_{\alpha=\pm} \left\{ F_{\text{id}}(V, T, n_\alpha) + \frac{k_{\text{B}}T}{2n_\alpha} \int_V [\Delta\rho_\alpha(\mathbf{r})]^2 \, \mathrm{d}\mathbf{r} \right\}, \qquad 24.$$

where $F_{\text{id}}(V, T, n_\alpha)$ is the Helmholtz free energy of an ideal gas of density n_α. The free energy functional defined by Equations 5 and 7, neglecting F_{corr}, is now a quadratic functional of the local densities, and the resulting Euler-Lagrange equation reduces to a linear multicenter PB (LPB) equation for the local potential $\psi(\mathrm{r})$, in the familiar form

$$\left(\nabla^2 - \kappa_{\text{D}}^2\right)\psi(\mathbf{r}) = -\frac{4\pi}{\epsilon}\rho^{\text{ext}}(\mathrm{r}). \qquad 25.$$

This linear equation is easily solved by Fourier transformation in the bulk, with the boundary condition that the potential and its gradient vanish at infinity. Because ρ^{ext} is a linear superposition of contributions from the N polyions, the same is true of $\psi(\mathrm{r})$ and the resulting $\rho_\alpha(\mathrm{r})$. Because microions cannot penetrate the spherical polyions, the excluded volume condition, $\rho_\alpha(\mathbf{r}) = 0$; $[\mathbf{r} - \mathbf{R_i}] < a(1 \le i \le N)$, must be imposed via a constraint, or by the use of a polyion-microion pseudo potential (45, 46). Note that, strictly speaking, the linear superposition of densities only holds provided the electric double layer associated with a given polyion does not overlap a neighboring polyion (weak overlap approximation). This is not a significant limitation except at high polyion packing fraction. The excluded volume condition leads to an additional polyion charge renormalization such that the effective charge Z^* is multiplied by the DLVO factor $e^{\kappa_{\text{D}}a}/(1 + \kappa_{\text{D}}a)$; the product is henceforth designated by Z^*. The local potential is finally of the form

$$\psi(\mathbf{r}) = \sum_{i=1}^{N} \Psi^{(i)}(\mathbf{r}) = \sum_{i=1}^{N} \frac{Z^* e}{\epsilon} \frac{\exp(-\kappa_{\text{D}}|\mathbf{r} - \mathbf{R_i}|)}{|\mathbf{r} - \mathbf{R_i}|}. \qquad 26.$$

When Equation 26 and the resulting $\rho_\alpha(\mathbf{r})$ are substituted into the quadratic free energy functional, the effective interaction energy Equation 8 between the N polyions reduces to

$$V_N(\{\mathbf{R_i}\}) = V_0 + \sum_{i<j} v(|\mathbf{R_i} - \mathbf{R_j}|), \qquad 27.$$

where $V_0(T, n, n_+, n_-)$ is a state-dependent "volume" term (80), the detailed expression of which is given elsewhere (46, 81). This term has been generally overlooked, but it strongly influences the calculated phase behavior of charge-stabilized colloidal dispersions, as discussed later. The main contribution to the volume term is the sum of cohesive electrostatic free energies arising from the electrostatic attraction between each polyion and its associated double layer of opposite charge. The physical interpretation of V_0 is discussed in detail elsewhere (82). The effective pair potential is precisely of the well known DLVO form (65), namely

$$v(R) = \frac{Z^{*2}e^2}{\epsilon}\frac{e^{-\kappa_D R}}{R}. \qquad 28.$$

Note that the pair-wise additivity in Equation 27 is a direct consequence of the quadratic nature of the approximate free energy functional; the exact ideal contribution (Equation 5) to the free energy would lead to many-body effective interactions.

There are alternative contraction procedures to reduce the initial asymmetric, multicomponent PM to an effective one-component system, based on the OZ equations and approximate closures, like the mean spherical approximations for the partial pair distribution functions $g_{\alpha\beta}(r)$ (10–13). The simple assumption of the asymptotic behavior $c_{\alpha\beta}(\mathrm{r}) \to -v_{\alpha\beta}(r)/k_\mathrm{B}T$ of the direct correlation functions is sufficient to show that the effective pair interaction is asymptotically of the DLVO form (28) and reduces to (28) in the appropriate limits. Corrections to the DLVO potential at short range may be obtained from numerical solutions of the fluid integral equations, and these confirm the purely repulsive nature of the effective pair potential at low colloid concentration, at least when all microions are monovalent (13).

The phase diagram of a monodisperse system of particles interacting via the DLVO pair potential (Equation 28) has been determined by extensive MC simulations as a function of colloid and salt concentrations, the latter determining the inverse Debye screening length κ_D (42, 43). As expected from the purely repulsive nature of the effective pair potential, the phase diagram exhibits a first-order transition between a single (disordered) fluid phase and (ordered) face-centered-cubic or body-centered-cubic crystalline phases, the latter being the stable phase in the $\kappa_\mathrm{D} \to 0$ limit, which corresponds to the widely studied one-component plasma model (83). However, the coarse-graining procedure leading from the initial multicomponent polyion/microion "mixture" to the effective one-component system also introduces the volume term V_0 into the effective interaction energy between polyions. Because V_0 is a nonlinear function of the polyion density n, due to the overall charge neutrality condition $nZ^* + n_+z_+ + n_-z_- = 0$, this term

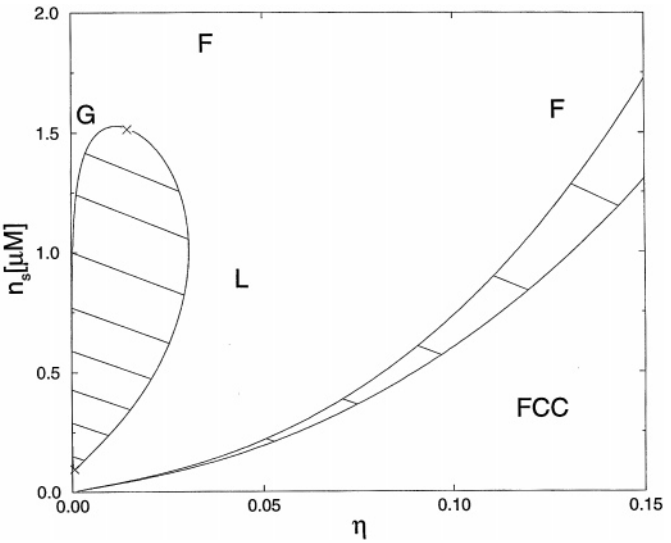

Figure 2 Phase diagram for a charged suspensions in the $\eta - n_s$ plane with $\eta = 4\pi n a^3/3$ and $Z = 350$, $a = 380$ nm, $\epsilon = 13.9$ (penthanol), and monovalent counterions at room temperature. Possible phases are fluid (F), gas (G), liquid (L), and face-centered-cubic (FCC) crystals. Tie lines denote coexistence conditions.

must be included in the free energy for a proper determination of the phase behavior (45, 46, 82). At high concentrations of added salt, the variation of V_0 with n is slow enough that it does not affect the phase behavior significantly. At salt concentrations lower than 10^{-5} M, the volume term drives a van der Waals–like instability of the fluid, which separates into two phases of very different colloid concentrations, reminiscent of the gas and liquid phases of ordinary molecular fluids. Depending on the effective colloid surface charge, this phase separation is completely disconnected from the freezing transition driven by the repulsive pair interaction (28), and it exhibits upper and lower critical points (reentrant behavior) in the $n - n_s$ plane, where s is salt (see Figure 2); or it merges with the freezing line, leading to a considerable broadening of the fluid-solid coexistence region, and the possibility of upper and lower triple points, as seen in Figure 3. The possibility of a fluid miscibility gap in polyelectrolytes had been conjectured in 1938 by Langmuir (84), who referred to it as unipolar coacervation, and the complex phase scenario discussed elsewhere (45, 46, 82) has recently been confirmed by an extension of Debye-Hückel theory to the highly asymmetric PM (85). These calculations provide a natural explanation for the observed phase behavior of charge-stabilized colloids, including the formation of voids (67–72), without the assumption of a long-range attractive component in the effective pair interaction, which is frequently made (86) but which lacks a firm theoretical basis.

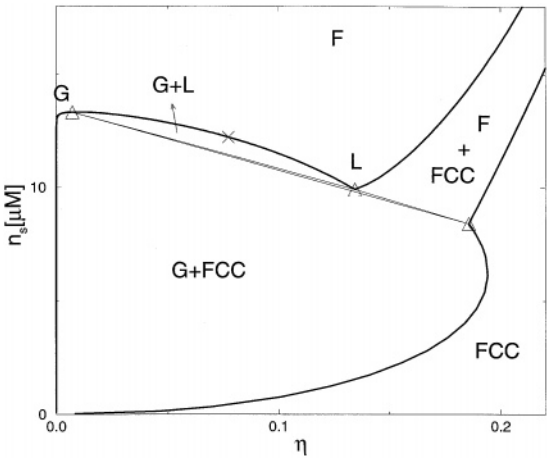

Figure 3 Same as Figure 2, but for $Z = 1000$, $a = 350$ nm, and $\epsilon = 25.3$ (ethanol). There is a triple point of coexisting gas, liquid, and crystal.

Beyond DLVO

It was shown earlier that the effective force between two uniformly charged plates may turn attractive at short distances if correlations between microions are properly accounted for. A similar effect is expected to hold between two spherical polyions, as first conjectured for two isolated spheres by Patey (15) on the basis of numerical solutions of the HNC equation. When two spheres are sufficiently close, such that the shortest separation h between their surfaces is much less than their radius a, the problem reduces essentially to that of two charged planes discussed earlier: A short-range correlation-induced attraction may be expected for divalent counterions. A collective polarization mechanism of adsorbed counterions operates in the opposite limit $h \gg a$ and leads to a "doubly screened" attractive component, proportional to $e^{-2\kappa_D R}$, which is always dominated by the DLVO repulsion (87). It is important to stress that effective attractions between spherical polyions require a finite concentration of the latter in the absence of salt, i.e. when only counterions are present (87, 88). No such restriction holds at finite salt concentration, where the problem of two isolated polyions is a meaningful limit.

A similar doubly screened attraction between spherical polyions occurs in the charge regulation PM introduced earlier (cf Equation 12) (27). Note that the effective interaction between two isolated colloids is purely attractive (for $R > 2a$) in the case of a symmetrical adsorption of co- and counterions ($V_+ = V_-$ in Equation 12), because the colloidal particles are then, on average, neutral.

Computer Simulations

Density-functional MD simulations were performed for monovalent counterions without (78, 89) and with (90) added salt. The effective interaction between the polyions was found to be repulsive and in quantitative agreement with DLVO

theory, provided the charge was renormalized according to the cell model prescription incorporating the excluded volume correction (91). This approach includes counterion correlations, but it is not completely equivalent to a full simulation of the PM because an approximate polyion-counterion pseudopotential is used and the exact density functional of the electrolyte is unknown. Because of the high charge asymmetry between poly- and microions, a full simulation of the PM requires the inclusion of many counter- and salt ions and is not feasible on present-day computers. There are two ways to escape from this: either by considering only a small number of polyions, or by reducing the charge asymmetry significantly. By considering only two polyions within the PM, the effective pair potential can be calculated within a simulation by averaging over the microscopic ions while keeping the polyion positions fixed. For monovalent microions, the simulation yields repulsive forces correctly described by DLVO theory both with (92) and without (93) added salt. For divalent counterions, attractive forces are obtained, which may be attributed to counterion correlations (88) and Coulomb depletion (94), resulting from a depletion zone of counterions between two nearly touching polyions due to the strong counterion repulsion. A typical snapshot of the counterions around two fixed polyions and the averaged force versus polyion distance are shown in Figure 4. A system of three polyions was simulated in order to extract effective triplet interactions, which were found, however, to be small with respect to the pair-wise part (95).

On the other hand, there are a number of full simulations of the PM with a reduced charge asymmetry corresponding to micellar rather than colloidal polyions. Most of the work is summarized in a review by Vlachy (96). As for more recent work, the role of salt valency has been investigated in some detail (97). Moreover, the charge asymmetry was pushed to $Z{:}z_+ = 60{:}1, 60{:}2, 60{:}3$ using efficient

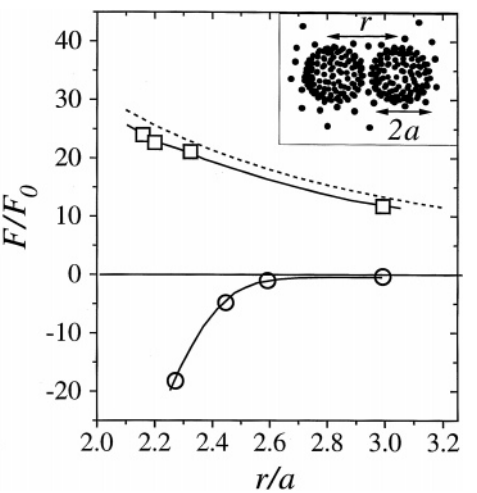

Figure 4 Effective force F in units of $F_0 = \frac{Z^2e^2}{a^2} \times 10^{-4}$ between two polyions versus reduced distance r/a. The squares are for aqueous suspensions. The force is repulsive in good agreement with DLVO-theory (*dashed line*). (*Circles*) Show attraction for a solvent with a strongly reduced dielectric constant ϵ. (The parameters are given in detail in Reference 94.) (*Inset*) A counterion configuration around two fixed polyions.

cluster move algorithms (14, 98) and treating 80 polyions simultaneously (99). For the 60:3 asymmetry, clear indications for a phase separation were reported, which can be attributed to an effective attraction between polyions.

POLYIONS IN CONFINED GEOMETRIES

The bulk behavior of polyionic dispersions is expected to change significantly in the presence of neutral or charged interfaces confining the dispersion to a restricted volume. Such confinement occurs naturally in the vicinity of the sample container, which may be approximated locally by an infinite plane restricting the suspension to a half space. Many experiments are carried out in a slit geometry, with the suspension confined between parallel planes (e.g. glass plates); if the interplanar spacing is comparable to the diameter $2a$ of the polyions, the suspension behaves like a quasi–two-dimensional many-body system exhibiting interesting phase behavior (100).

The electrostatic effects of confinement are essentially threefold. (*a*) The interface between two different dielectric media, e.g. the suspension and the glass of the container wall, must be characterized by appropriate boundary conditions; in particular the dielectric discontinuity implies the presence of electrostatic image charges. (*b*) The confining surfaces lead to a reduction in screening power of the electrolyte, which ceases to be exponential in directions parallel to the surface (101). (*c*) If the surfaces are charged, they attract or repel the polyions and microions and release additional counterions into the suspension.

These effects will modify the electrostatic interactions between double layers associated with polyions close to the confining walls. This has been clearly demonstrated by a number of direct measurements of the effective forces between spherical polyions confined near a glass wall, or in narrow slits, using digital video microscopy techniques similar to those mentioned earlier for measurements in the bulk. Measurements of the colloid pair distribution function $g(r)$ carried out at sufficiently low concentration allow the effective pair potential to be extracted directly from Equation 23 (102, 103), whereas data collected from more concentrated samples, where the effective potential $v(r)$ is expected to differ significantly from the potential of mean force defined by Equation 23, require an elaborate inversion procedure based on fluid integral equations (properly adapted to a two-dimensional geometry) (104, 105), or on an iterative method involving computer simulations (102). These experiments leave little doubt of the existence of an attractive component of the effective polyion pair potential at low ionic strength (i.e. for salt concentrations estimated to be below about 10^{-5} M), when the polyions are highly confined, as achieved in narrow slits (102, 104), or by localizing them close to a single plane by optical tweezers (103, 106, 107). The observed attractive well in $v(r)$ is relatively shallow (depth of the order of k_BT) and long ranged; typically, $v(r)$ becomes negative for interparticle distances considerably larger than the particle diameter $2a$. The experiments carried out for two particles close to a

charged plate with the center-to-center vector parallel to the plate clearly show that the attractive well disappears when the particles are moved away from the plate; the measured $v(r)$ returns to its bulk DLVO form (Equation 28) when the distance to the plate is several particle diameters (103, 106, 107). An additional twist for suspensions of colloidal particles confined to a slit is provided by the introduction of quenched obstacles, in the form of larger, charged colloids, which form a disordered porous two-dimensional matrix. As the concentration of such obstacles is increased, the effective interaction potential between the smaller colloids is observed to develop a second attractive component extending to larger interparticle separations (108). Closely related observations of metastable colloidal crystallites suggest that facets of such crystals behave very much like charged plates, inducing effective attractions between nearby polyions (106) due to many-body interactions.

The DFT formulation of DLVO theory in the bulk has been extended to the case of confined particles. The electrostatic potential due to a point polyion near a planar surface separating two media of dielectric constants ϵ and ϵ' was determined within LPB theory by Stillinger as early as 1961 (109). The case of two spherical polyions of finite radius a near an uncharged planar surface was examined within LPB theory (110). Because microions cannot leak beyond the dividing surface, the spherical symmetry of the electric double layers around each of the polyions is broken. The effective repulsion between the polyions is enhanced and decays like $1/R^3$, where R is the separation parallel to the surface, as expected from the considerations of Jancovici (101).

If the confining surface carries an electric charge density σ, as would be the case for a glass plate in contact with an aqueous dispersion, the planar electric double layer building up near the surface will modify the local co- and counterion concentrations in the vicinity of nearby polyions and, hence, influence their mutual interaction. Considering the charged wall as an additional colloidal particle of infinite radius, it is clear from the inherent pair-wise additivity that the quadratic free energy functional, defined by Equations 24 and 7 (with $F_{\text{corr}} = 0$), which underlies LPB theory, will not affect the effective interaction between two polyions near the wall. Clearly the intrinsic three-body nature of the problem must be taken into account. The minimal theory to achieve this is to carry the expansion in Equation 24 one order further, allowing for a direct coupling between the three double layers associated with the polyions and surface. Application of DFT perturbation theory (78) leads to the prediction of a long-range attraction between polyions, decaying like $1/R^3$ along the surface and exponentially normal to the surface, for finite concentrations of polyions, to allow for an imbalance between co- and counterion concentrations (111). Both the location and depth (typically on the order of $k_{\text{B}}T$) of the predicted potential well are in semiquantitative agreement with direct experimental measurements (103, 106, 107). The attraction predicted within mean-field theory occurs when the surfaces of the spherical polyions are several Debye lengths apart, and it has nothing to do with the correlation-induced attraction at very short range predicted in the bulk, and which is significant only for multivalent counterion (87, 88, 94, 99, 97).

The generalization of DLVO theory may also be extended to slit (112, 113) and pore (114) geometries. The quasi–one-dimensional confinement in the latter case leads to an even slower decay of the long-range attraction. The existence of an effective attraction between two like-charged polyions confined by a charged cylindrical surface was also predicted on the basis of numerical solutions of the nonlinear PB equation (115), but it has since been proved rigorously that PB theory can only lead to purely repulsive effective interaction between two identical polyions confined to a cylinder of arbitrary cross section (116, 117), whatever the boundary conditions at the charged surfaces. This proof does not invalidate the results of the perturbation theory (111, 113, 114) because charge renormalization (which accounts for short-range correlations), followed by an LPB perturbation treatment of the nonadsorbed counterions, is not a mere approximation to nonlinear PB theory, which is, moreover, unphysical near highly charged surfaces.

A direct simulation of the PM for confined colloids is only feasible for low surface charges and small particle sizes (118). In this regime, the attraction between colloids is strongly enhanced by the presence of a charged wall with respect to that in the bulk (94). Also, the wall-particle interaction was found (118) to be attractive for divalent counterions.

ROD-LIKE POLYIONS

There is a large variety of rod-like polyions ranging from synthetic suspensions to biological macromolecules. These include colloidal β-FeOOH (119), imogolite (120), boehmite (121–123), polytetrafluoroethylene (124), ellipsoidal polystyrene latex particles (125), and cylindrical micellar aggregates (126, 127), as well as virus solutions from tobacco-mosaic virus (128, 129), bacterial fd (130, 131), and Pf1 viruses (132). Another motivation to study rod-like colloids comes from the self-assembly of charged stiff biopolymers such as DNA strands (133, 134), F-actin fibers (135), and microtubules (135), which constitute rod-like polyions on a supramolecular rather than a colloidal length scale.

The simplest model system is the electric double layer around a single, infinitely long, cylindrical polyion of radius a that is homogeneously charged with line charge density λ. LPB theory leads to the electric potential $\Psi(r) = \lambda K_0(\kappa_D r)/aK_1(\kappa_D a)\epsilon$, where r is the distance from the rod axis and $K_0(x)$, $K_1(x)$ are Bessel functions of imaginary argument. Consequently, LPB theory predicts the effective interaction $v(r)$ between two parallel rods per unit length to be of the following form:

$$v(r) = \frac{\lambda^2}{(\kappa_D a K_1(\kappa_D a))^2 \epsilon} K_0(\kappa_D r), \qquad 29.$$

where the factor $1/[\kappa_D a K_1(\kappa_D a)]$ is the excluded volume correction. Contrary to the three-dimensional case, PB theory can be solved analytically within a cylindrical cell around the charged rod for vanishing salt concentration (18, 136). The

analytical solution for the counterion density field around the colloidal rod exhibits a strong peak at contact (137), providing a theoretical framework of Manning counterion condensation (138, 139). As for spherical macroions, one cannot extract an effective interaction from the PB solution for a single double layer directly. One possibility is to proceed as for the spherical PB cell model. Matching the LPB theory at the cell boundary (140), one derives the effective interaction potential $v(r) = \lambda^{*2}/\epsilon K_0(\kappa r)$ where κ and λ^* are renormalized according to the cell model prescription.

A more direct theory, which requires a larger numerical effort, is to solve the two-dimensional PB theory for two parallel rods in a slit geometry and extract the effective force from there. In a recent numerical study (141) no attraction was found, consistent with the exact result (116, 117) in three dimensions.

Beyond the PB level of description, computer simulations for the effective interaction between two parallel, homogeneously charged rods have been performed for divalent counterions and no added salt (142). An effective attraction between the rods was found. The question is whether the attraction is due to correlations (143) or to fluctuations (144, 145). If the former is true, the attraction should increase with decreasing temperature and may even persist for zero temperature, whereas fluctuation-induced attraction should increase with temperature. A simple model (146) gave significant support for a correlation picture. This can be intuitively understood as the gain in electrostatic energy on bringing together staggered arrays of adsorbed counterions (60, 147). Fluctuation (148, 149) and polarization effects (150) may still play an important additional role. For parallel rods on a triangular lattice, a negative pressure was found by computer simulation with divalent counterions (151), which can be attributed to some attractive component in the effective interactions.

Qualitatively, the situation closely resembles the case of spherical macroions. But there are also differences. First, Manning condensation theory applies only to rod-like polyions. A possible mechanism of attraction of nearly touching rods by sharing Manning-condensed counterions was proposed, which is only possible for rods (152). Second, the Coulomb depletion mechanism for attraction (94) was found to be irrelevant for parallel rods.

For finite rod lengths and arbitray orientations of the rods, the effective interaction between two rods will depend both on the rod orientations and on their center-of-mass separation. Starting from point charges distributed along the rods, LPB theory results in a Yukawa-segment model (153), which was confirmed by density-functional MD simulations for monovalent counterions (140), provided the charge and the screening constant κ are renormalized according to the cell model prescription. The associated phase diagram for parameters suitable for the TMV suspension was calculated, involving different liquid crystalline phases (154).

A full simulation of the PM was performed for stiff polyelectrolytes (155), resulting in bundle formation, which is a possible sign of an effective attraction. Clearly, the effective pair potential picture is insufficient for bundles (156), and many-body interactions play a significant role (148, 149).

LAMELLAR POLYIONS

Lamellar polyions may be schematically looked on as rigid or flexible charged surfaces or platelets, providing a two-dimensional counterpart of charged rods or polyelectrolytes. Examples are the geologically and technologically important smectite clays (157) and self-assembled bilayers of ionic surfactants, which constitute the prototype of biological membranes (51).

Consideration is first given to electric double layers around infinitely thin, uniformly charged circular or square platelets, which constitute a reasonable model of smectite clay particles, and in particular of the widely studied synthetic Laponite mineral particles. To a good approximation the latter are rigid, thin disks of thickness $d \approx 1$ nm and radius $a \approx 15$ nm, carrying a structural surface charge $\sigma \approx -e/(\text{nm})^2$. Natural montmorrilonite clays are silicate mineral platelets of similar chemical composition and crystal structure, but of irregular and polydisperse shape, and of much larger lateral dimension, implying some degree of bending flexibility.

Dry powders of clay will swell on addition of water, releasing counterions into the interlamellar volume and building up interacting electric double layers; the swelling is essentially driven by the double-layer repulsion of mostly entropic origin. During the initial stages of swelling, the spacing h between platelets remains small compared with their lateral extension, so that a moderately swollen lamellar phase may be reasonably modeled by a stack of infinite charged planes (158). The results for planar geometry, discussed earlier, apply then directly to the swollen phase. In particular, limited swelling, often observed in the presence of divalent counterions, may be related to the cohesive behavior (effective attraction between planes, or negative disjoining pressure) due to correlation effects within the PM (159). An important issue in the understanding of the swelling behavior is the competitive condensation of counterions of different valence and/or size (159, 160). The PM model is, however, expected to be inadequate when the interlamellar spacing h is only on the order of a few microion diameters. Under those conditions, the molecular nature of the solvent (water) must be explicitly taken into account. Constant-pressure MC simulations clearly show the importance of counterion hydration in determining the swelling behavior, and point to the role of K^+ ions as a clay-swelling inhibitor (161). When swelling proceeds until the interlamellar spacing h becomes comparable to the platelet radius a, finite-size (edge) effects become important. The force acting on a platelet follows from the integration of the stress tensor $\underline{\underline{\Pi}}$ over the two faces Σ_+ and Σ_- of the platelet:

$$\mathbf{F} = -\int_{\Sigma_+,\Sigma_-} \underline{\underline{\Pi}}\, \mathrm{d}\mathbf{s}, \qquad 30.$$

where $\mathrm{d}\mathbf{s} = \hat{\mathbf{n}}\mathrm{d}s$ is the surface element oriented along the outward normal $\hat{\mathbf{n}}$, and

the stress tensor has the standard form

$$\underline{\underline{\Pi}} = \left[P(\mathbf{r}) + \frac{\epsilon}{8\pi} |\mathbf{E}|^2 \right] \mathbf{I} - \frac{\epsilon}{4\pi} \mathbf{E}(\mathbf{r}) \otimes \mathbf{E}(\mathbf{r}), \qquad 31.$$

which generalizes the uniaxial expression (Equation 20). Within LPB theory, Equation 30 leads to the following expression for the force between two coaxial disks separated by h, immersed in an ionic solution of inverse Debye length κ_D (162):

$$F_z(h) = (\pi a^2) \times \frac{4\pi\sigma^2}{\epsilon} \int_0^\infty J_1^2(x) \frac{1}{x} \exp\left\{ -\frac{h}{a} \sqrt{x^2 + \kappa_D^2 a^2} \right\} \mathrm{d}x. \qquad 32.$$

Numerical solutions of the nonlinear PB equation, for the same coaxial geometry, show that the LPB expression (32) strongly overestimates the force (163), as in the spherical case, thus requiring a proper renormalization of the surface-charge density σ. Recent MC simulations show that the force may become attractive for divalent counterions, as in the case of infinite charged planes, but that the finite size of the disks leads to significant differences in the relative weight of electrostatic and contact contributions (164).

Finite concentration effects in highly swollen stacks of parallel platelets of finite size may be examined within a cell model, compatible with the shape of the platelet. A coaxial cylindrical cell is chosen for a disk-shaped platelet, whereas a parallelepipedic cell is better adapted to square platelets (162, 165). Note that the platelet concentration determines the cell volume, but not the aspect ratio of the cell, e.g. the ratio R/h in the case of a cylindrical cell of radius R and height h equal to the interlamellar spacing; the optimum aspect ratio for a given volume and electrolyte concentration is determined by minimizing the free energy of the microions in the cell. The latter has been calculated within LPB theory, which can be solved analytically (162, 165), and within nonlinear PB theory, which requires numerical solution; the latter is greatly simplified within a Green's function formulation (163, 166).

The osmotic pressures calculated as a function of Laponite concentration within PB theory agree reasonably well with experimental data (167) for reservoir salt concentrations on the order of 10^{-3} M or larger, but differ dramatically from the predictions of one-dimensional PB theory for stacks of infinite platelets, pointing to the importance of edge effects in highly swollen clays (166).

In very dilute dispersions of clay platelets, such that the distance between the centers of neighboring polyions is significantly larger than the particle radius, the platelets can rotate more or less freely (sol phase). As the concentration increases, a gel phase is formed, depending on salt concentration. Several recent experiments have attempted to establish a link between the mesoscopic fractal structure of the gel and its rheological properties (167–169), but due to metastability and aging of the dispersions (170), no clear-cut scenario has yet emerged.

A theoretical description of the sol-gel transition of clay dispersions hinges on a knowledge of the highly anisotropic effective interaction between charged platelets in an electrolyte. The charged segment, or site-site model, introduced earlier for

charged rods has been generalized to charged circular platelets, and used in MD simulations of Laponite dispersions (171).

For well-separated platelets, the effective pair potential reduces to a sum of screened interactions between the electrostatic multipoles associated with the anisotropic electric double layers around each platelet (172). A simplified version of such an effective interaction, involving infinitely thin disks carrying an unscreened quadrupole moment, has been used in MC simulations that predict a reversible sol-gel transition (173).

Lipid bilayers and membranes constitute another class of lamellar polyions, which are flexible. Electrostatic interactions renormalize the bending rigidity of these flexible membranes (51), a subject of ongoing work beyond the scope of this review. In relation to the correlation-induced attraction between like-charged planes discussed earlier, the fluidity of membranes provides an additional mechanism for attraction between membranes, resulting from the lateral charge fluctuations within the planes of the latter (174).

DISCRETE SOLVENT EFFECTS

So far, all theoretical considerations of interacting electric double layers have been based on the PM, which ignores the molecular nature of the solvent. The PM thus neglects excluded volume effects of the latter, as well as hydration of ions and the expected reduction of the local dielectric constant near highly charged surfaces, due to polarization of nearby water molecules. Neglect of these and other solvent effects is expected to be particularly inadequate in situations where the spacing between two charged polyion surfaces is only on the order of a few molecular diameters.

To go beyond the PM level of description, simple models have been used to describe the solvent molecules (generally water). The crudest model is to represent the latter by neutral hard spheres of appropriate diameter while keeping a macroscopic dielectric constant ϵ in the Coulombic interactions between ions; this model accounts only for excluded volume effects. The next refinement is to consider hard spheres with embedded point dipoles, to account for the highly polar nature of the solvent (8, 175), whereas a reasonable local coordination of the solvent molecules can only be achieved by adding higher-order multipoles (176–178). In MC or MD simulations, much more sophisticated pair potentials may be used, involving three or more interaction sites on each water molecule, as in the widely used SPC/E potential (179).

A purely hard sphere (HS) solvent is implicit in the modified PB formulation of Kralj-Iglič & Iglič (180) and others (114, 181). As expected, the modified PB equation leads to a saturation of the counterion density at contact for high surface-charge densities. The force between two charged surfaces in a mixture of charged and neutral hard spheres was calculated by Tang et al (182) within a DFT

generalizing the earlier theory of the same authors for a PM electrolyte (59); the force is a strongly oscillatory function of the spacing between the plates, due to HS layering, and is insensitive to surface charge and salt concentration. The latter observation, which holds when solvent, anions, and cations are of the same size, does not carry over to the more realistic case of unequal diameters, which has been investigated within inhomogeneous HNC theory (183). At low surface charge, the total force between platelets is reasonably approximated by a superposition of the pure HS solvent "hydration" force, and the electrostatic contribution of the ions, as calculated within the PM, in the case of equal diameters (183, 184).

The dipolar HS model for the solvent was first used to determine the structure of the electric double layer near a single charged wall within the mean spherical approximations (185, 186). More accurate and complete results on the planar electric double layer in a dipolar solvent were obtained from numerical solutions of the coupled reference HNC equations for the three density profiles (187). These calculations give statistical mechanics evidence for the reduction of the local dielectric constant near the charged surface, and for significant electrostriction. A generic density functional, based on the successful "fundamental measure" theory for hard core fluids of Rosenfeld et al (188, 189), has been put forward, which can be adapted to any polyion geometry (190); when applied to a single planar double layer, this theory shows a considerable enhancement of the counterion density at contact, when a dipolar, rather than bare HS solvent is used.

The effective solvation force between two charged plates immersed in an ionic solution of charged and dipolar HS was calculated within a quadratic free energy functional of the local density, charge density, and polarization, generalizing Equations 24 and 6 (with direct correlation functions approximated by bulk mean-spherical-approximations solutions) (191). This calculation provided the first convincing evidence of the strong influence of a granular (as opposed to continuous) solvent on the solvation forces at short range.

The most complete investigation so far of the potential of mean force between two spherical polyions immersed in an ionic solution with a "realistic" solvent involving hard spheres with point dipoles and tetrahedral quadrupoles (177) appears to be the work by Kinoshita et al (192), who solved the reference HNC equations for this highly asymmetric multicomponent mixture, for ratios $10 \leq a/a_s \leq 30$, where a and a_s are the polyion and solvent molecule radii, respectively. While maintaining a_s fixed at 0.14 nm, a value appropriate for water, these authors varied the counterion radius. Their most striking finding is that larger counterions are more strongly adsorbed to the polyion in the presence of a molecular solvent, leading to a greater reduction of the Coulomb repulsion between the polyions, and even to the possibility of an effective attraction for monovalent counterions, when their radius exceeds a_s by more than 20%. The trend toward a reduction of effective repulsion with increasing counterion size is the exact opposite of the prediction of the PM, a clear illustration of the pitfalls of the latter in describing the short-range behavior of solvation forces!

OUTLOOK

Although the understanding of effective interactions between electric double layers has clearly advanced in the past decade through a combination of new theoretical approaches, quantitative measurements, and large-scale computer simulations, there are still many open questions. Future research should focus on the influence of image charges (193) due to dielectric discontinuities between the solvent and the container walls or the polyions themselves. Real samples possess, moreover, an intrinsic polydispersity in size, charge, and shape, which becomes relevant for a quantitative comparison between theory and experimental data. Another rapidly growing field concerns flexible polyelectrolyte chains whose stiffness is governed by their persistence length (137). A theoretical approach needs input from both nonlinear screening and polymer theories. The microscopic incorporation of the solvent is still in its early stage, and full molecular theories describing hydration forces and hydrogen bonding are highly desirable for aqueous suspensions. Lastly, alternative approaches, such as recent field theoretical formulations (194), might lead to additional insight.

ACKNOWLEDGMENTS

We thank E Allahyarov, D Goulding, Y Levin, P Linse, V Lobaskin, P Pincus, and R van Roij for helpful comments.

LITERATURE CITED

1. Israelachvili J. 1992. *Intermolecular and Surface Forces*. London: Academic. 2nd ed.
2. Chen SH. 1986. *Annu. Rev. Phys. Chem.* 37:351
3. Evans R. 1991. See Ref. 195, pp. 85–175 York: Dekker
4. Carnie SL, Torrie GM. 1987. *Adv. Chem. Phys.* 56:141
5. Blum L, Henderson D. 1991. See Ref. 195, pp. 239–76
6. Attard P. 1996. *Adv. Chem. Phys.* 92:1
7. Arora AK, Tata BVR, eds. 1996. *Ordering and Phase Transitions in Charged Colloids*. New York: VCH
8. Hansen JP, McDonald IR. 1986. *Theory of Simple Liquids*. London: Academic. 2nd ed.
9. Belloni L. 1985. *Chem. Phys.* 99:43
10. Belloni L. 1986. *J. Chem. Phys.* 85:519
11. Belloni L. 1988. *J. Chem. Phys.* 88:5143
12. Khan S, Morton T, Ronis D. 1987. *Phys. Rev. A* 35:4295
13. González-Mozuelos P, Carbajal-Tinoco MD. 1998. *J. Chem. Phys.* 109:11074
14. Lobaskin V, Linse P. 1999. *J. Chem. Phys.* 111:4300
15. Patey GN. 1980. *J. Chem. Phys.* 72:5763
16. Wu J, Bratko D, Prausnitz JM. 1998. *Proc. Natl. Acad. Sci. USA* 95:15169
17. Gouy G. 1910. *J. Phys.* 9:457
18. Fuoss RM, Katchalsky A, Lifson S. 1951. *Proc. Natl. Acad. Sci. USA* 37:579
19. Marcus RA. 1955. *J. Chem. Phys.* 23:1057
20. Rosenfeld Y, Schmidt M, Löwen H, Tarazona P. 1997. *Phys. Rev.* E55:4245
21. Kjellander R, Marčelja S. 1988. *J. Chem.*

Phys. 88:7129; Erratum. 1988. *J. Chem. Phys.* 89:7649
22. Alexander S, Chaikin PM, Grant P, Morales GJ, Pincus P, Hone D. 1984. *J. Chem. Phys.* 80:5776
23. Groot RD. 1991. *J. Chem. Phys.* 95:9191
24. Stevens MJ, Falk ML, Robbins MO. 1996. *J. Chem. Phys.* 104:5209
25. Gisler T, Schulz SF, Borkovec M, Sticher H, Schurtenberger P, et al. 1994. *J. Chem. Phys.* 101:992
26. Ninham BW, Parsegian VA. 1971. *J. Theor. Biol.* 31:405
27. Belloni L, Spalla O. 1997. *J. Chem. Phys.* 107:465
28. von Grünberg HH. 1999. *J. Colloid Interface Sci.* 219:339
29. Härtl W, Versmold H, Wittig U. 1992. *Langmuir* 8:2885
30. Lutterbach N, Versmold H, Reus V, Belloni L, Zemb T. 1999. *Langmuir* 15:337
31. Lutterbach N, Versmold H, Reus V, Belloni L, Zemb T, Lindner P. 1999. *Langmuir* 15:345
32. Belloni L. 1998. *Colloids Surf. A* 140:227
33. Levin Y, Fisher ME. 1996. *Physica A* 225:164
34. Tamashiro MN, Levin Y, Barbosa MC. 1998. *Physica A* 258:341
35. Kjellander R, Mitchell DJ. 1994. *J. Chem. Phys.* 101:603
36. Kjellander R, Mitchell DJ. 1997. *Mol. Phys.* 91:173
37. Stillinger FH, Lovett R. 1968. *J. Chem. Phys.* 48:3858
37a. Stillinger FH, Lovett R. 1968. *J. Chem. Phys.* 49:1991
38. Attard P. 1993. *Phys. Rev.* E48:3604
39. Leote de Carvalho RJF, Evans R. 1994. *Mol. Phys.* 83:619
40. Kjellander R, Ulander J. 2000. See Ref. 196. In press
41. Attard P. 1995. *J. Phys. Chem.* 99:14174
42. Robbins M, Kremer K, Grest GS. 1988. *J. Chem. Phys.* 88:3286
43. Hamaguchi S, Farouki RT, Dubin DHE. 1996. *J. Chem. Phys.* 105:7641
44. Palberg T, Mönch W, Bitzer F, Piazza R, Bellini T. 1995. *Phys. Rev. Lett.* 74:4555
45. van Roij R, Hansen JP. 1997. *Phys. Rev. Lett.* 79:3082
46. van Roij R, Dijkstra M, Hansen JP. 1999. *Phys. Rev.* E59:2010
47. Yamanaka J, Yoshida H, Koga T, Ise N, Hashimoto T. 1998. *Phys. Rev. Lett.* 80:5806
48. Yoshida H, Yamanaka J, Koga T, Koga T, Ise N, Hashimoto T. 1999. *Langmuir* 15:2684
49. Kjellander R, Åkesson T, Jönsson B, Marčelja S. 1992. *J. Chem. Phys.* 97: 1424
50. Guldbrand L, Jönsson B, Wennerström H, Linse P. 1984. *J. Chem. Phys.* 80:2221
51. Andelman D. 1995. In *Structure and Dynamics of Membranes*, ed. R Lipowsky, E Sackmann, pp. 603–42. Amsterdam: Elsevier
52. Attard P, Mitchell DJ, Ninham BW. 1988. *J. Chem. Phys.* 89:4358
53. Oosawa F. 1968. *Biopolymers* 6:1633
54. Valleau JP, Irkov R, Torrie GM. 1991. *J. Chem. Phys.* 95:520
55. Pellenq RJM, Caillol JM, Delville A. 1997 *J. Phys. Chem.* B101:8584
56. Greberg H, Kjellander R, Åkesson T. 1997. *Mol. Phys.* 92:35
57. Greberg H, Kjellander R. 1998. *J. Chem. Phys.* 108:2940
58. Stevens MJ, Robbins MO. 1990. *Europhys. Lett.* 12:81
59. Tang Z, Scriven LE, Davis HT. 1992. *J. Chem. Phys.* 97:9258
60. Rouzina I, Bloomfield VA. 1996. *J. Phys. Chem.* 100:9977
61. Sjöström L, Åkesson T, Jönsson B. 1996. *Ber. Bunsenges. Phys. Chem.* 100:889
62. Borukhov I, Andelman D, Orland H. 1998. *J. Phys. Chem.* B.103:5042
63. Kékicheff P, Marčelja S, Sender TJ, Shubin VE. 1993. *J. Chem. Phys.* 99:6098
64. Hachisu S, Kobayashi Y, Kose A. 1973. *J. Colloid Interface Sci.* 42:2
65. Verwey EJW, Overbeek JTG. 1948. *Theory*

of Stability of Lkyophobic Colloids. Amsterdam: Elsevier.
66. Yamanaka J, Yoshida H, Koga T, Ise N, Hashimoto T. 1999. *Langmuir* 15:4198
67. Dosho S, Ise N, Ito K, Iwais S, Kitano H. et al. 1993. *Langmuir* 9:394
68. Tata BVR, Yamahara E, Rajamani PV, Ise N. 1997. *Phys. Rev. Lett.* 78:2660
69. Ito K, Yoshida H, Ise N. 1994. *Science* 263:66
70. Ise N, Konishi T, Tata BVR. 1999. *Langmuir* 15:4176
71. Palberg T, Wurth M. 1994. *Phys. Rev. Lett.* 72:786
72. Tata BVR, Rajalakshmi M, Arora AK. 1992. *Phys. Rev. Lett.* 69:3778
73. Vondermassen K, Bongers J, Mueller A, Versmold H. 1994. *Langmuir* 10:1351
74. Crocker JC, Grier DG. 1994. *Phys. Rev. Lett.* 73:352
75. Weiss JW, Larsen AE, Grier DG. 1998. *J. Chem. Phys.* 109:8659
76. Dufresne ER, Grier DG. 1999. *J. Chem. Phys.* 110:8845
77. Löwen H, Madden PA, Hansen JP. 1992. *Phys. Rev. Lett.* 68:1081
78. Löwen H, Hansen JP, Madden PA. 1993. *J. Chem. Phys.* 98:3275
79. Fushiki M. 1992. *J. Chem. Phys.* 97:6700
80. Grimson MJ, Silbert M. 1991. *Mol. Phys.* 74:397
81. Graf H, Löwen H. 1998. *Phys. Rev.* E57:5744
82. Van Roij R, Evans R. 1999. *J. Phys. Condens. Matter.* 11:10047
83. Baus M, Hansen JP. 1980. *Phys. Rep.* 59:1
84. Langmuir I. 1938. *J. Chem. Phys.* 6:873
85. Warren PB. 2000. *J. Chem. Phys.* In Press
86. Sogami I, Ise N. 1984. *J. Chem. Phys.* 81:6320
87. Levin Y. 1999. *Physica A* 265:432
88. Grønbech-Jensen N, Beardmore KM, Pincus P. 1998. *Physica A* 261:74
89. Tehver R, Ancilotto F, Toigo F, Koplik J, Banavar JR. 1999. *Phys. Rev.* E59:R1335
90. Löwen H, Kramposthuber G. 1993. *Europhys. Lett.* 23:673
91. Löwen H, D'Amico I. 1997. *J. Phys. Condens. Matter* 9:8879
92. D'Amico I, Löwen H. 1997. *Physica A* 237:25
93. Allahyarov E, Löwen H, Trigger S. 1998. *Phys. Rev. Lett.* 57:5818
94. Allahyarov E, D'Amico I, Löwen H. 1998. *Phys. Rev. Lett.* 81:1334
95. Löwen H, Allahyarov E. 1998. *J. Phys. Condens. Matter* 10:4147
96. Vlachy V. 1999. *Annu. Rev. Phys. Chem.* 50:145
97. Wu JZ, Bratko D, Blanch HW, Prausnitz JM. 1999. *J. Chem. Phys.* 111:7084
98. Linse P. 1999. *J. Chem. Phys.* 110:3493
99. Linse P, Lobaskin V. 1999. *Phys. Rev. Lett.* 83:4208
100. Grier DG, Murray CA. 1996. See Ref. 7, pp. 69–100
101. Jancovici B. 1982. *J. Stat. Phys.* 29:263
102. Kepler GM, Fraden S. 1994. *Phys. Rev. Lett.* 73:356
103. Crocker JC, Grier DG. 1996. *Phys. Rev. Lett.* 77:1897
104. Carbajal-Tinoco MD, Castro-Román F, Arauz-Lara JL. 1996. *Phys. Rev.* E53:3745
105. Rao KS, Rajagopalan R. 1998. *Phys. Rev.* E57:3227
106. Larsen AE, Grier DG. 1997. *Nature* 385:230
107. Grier DG. 2000. *J. Phys. Condens. Matter.* In press
108. Cruz de León G, Saucedo-Wolario JM, Arauz-Lara JL. 1998. *Phys. Rev. Lett.* 81:1122
109. Stillinger FH. 1961. *J. Chem. Phys.* 35:1584
110. Goulding D, Hansen JP. 1998. *Mol. Phys.* 95:649
111. Goulding D, Hansen JP. 1999. *Europhys. Lett.* 46:407
112. Denton AM, Löwen H. 1998. *Thin Solid Films* 330:7
113. Goulding D, Hansen JP. 1999. In *New Approaches to Problems in Liquid State Theory*, ed. C Caccamo, JP Hansen, G

Stell, pp. 321–36. Dordrecht, Netherlands: Kluwer
114. Hansen JP, Goulding D, van Roij R. 2000. See Ref. 196. In press
115. Bowen WR, Sharif AO. 1998. *Nature* 393:663
116. Neu JC. 1999. *Phys. Rev. Lett.* 82:1072
117. Sader JE, Chan DYC. 1999. *J. Colloid Interface Sci.* 213:268
118. Allahyarov E, D'Amico I, Löwen H. 1999. *Phys. Rev.* E60:3199
119. Maeda Y, Hachisu S. 1983. *Colloid Surf.* 6:1
120. Donkai N, Inagaka H, Kajiwara K, Urakawa H, Schmidt M. 1985. *Macromol. Chem.* 186:2623
121. Bugosh J. 1961. *J. Phys. Chem.* 65: 1791
122. Buining PA, Pathmamanoharan C, Jansen JBH, Lekkerkerker HNW. 1991. *J. Am. Ceram. Soc.* 74:1303
123. Wierenga AM, Philipse AP, Reitsma EM. 1997. *Langmuir* 13:6947
124. Folda T, Hoffmann H, Chanzy H, Smith P. 1988. *Nature* 333:55
125. Nagy M, Keller A. 1989. *Polym. Commun.* 30:133
126. Hendrikx Y, Charvolin J, Raviso M, Liébert MC, Holmes J. 1983. *Phys. Chem.* 87:3991
127. Wu CF, Chen SH, Shih LB, Lin JS. 1988. *Phys. Rev. Lett.* 61:645
128. Bawden FC, Pirie NW, Bernal JD, Fankuchen I. 1936. *Nature* 138:1051
129. Fraden S, Hurd AJ, Meyer RB, Cahoon M, Caspar DLD. 1985. *J. Phys. Colloq. C* 3:85
130. Graf C, Kramer H, Deggelmann M, Hagenbüchle M, Johner C, et al. 1993. *J. Chem. Phys.* 98:4920
131. Dogic Z, Fraden S. 1997. *Phys. Rev. Lett.* 78:2417
132. Booy FP, Fowler A. 1985. *Int. J. Biol. Macromol.* 7:327
133. Podgornik R, Strey HH, Parsegian VA. 1998. *Curr. Opin. Colloid Interface Sci.* 3:534
134. Strey HH, Podgornik R, Rau DC, Parsegian VA. 1998. *Curr. Opin. Struc. Biol.* 8:309
135. Tang JX, Wong SE, Tran PT, Janmey PA. 1996. *Ber. Bunsenges. Phys. Chem.* 100:1
136. Alfrey T, Berg PW, Morawetz H. 1951. *J. Polym. Sci.* 7:543
137. Barrat JL, Joanny J-F. 1996. *Adv. Chem. Phys.* 94:1
138. Manning GS. 1996. *Physica A* 231:236
139. Deserno M, Holm C, May S. 1999. *Macromolecules* 33:199
140. Löwen H. 1994. *J. Chem. Phys.* 100:6738
141. Ospeck M, Fraden S. 1998. *J. Chem. Phys.* 109:9166
142. Grønbech Jensen N, Mashl RJ, Bruinsma RF, Gelbart WM. 1997. *Phys. Rev. Lett.* 78:2477
143. Levin Y, Arenzon JJ, Stilck JF. 1999. *Phys. Rev. Lett.* 83:2680
144. Ha BY, Liu AJ. 1999. *Phys. Rev. Lett.* 83:2681
145. Ha BY, Liu AJ. 1997. *Phys. Rev. Lett.* 79:1289
146. Arenzon JJ, Stilck JF, Levin Y. 1999. *Eur. Phys. J.* B 12:79
147. Shklovskii BI. 1999. *Phys. Rev. Lett.* 82:3268
148. Ha BY, Liu AJ. 1999. *Europhys. Lett.* 46:624
149. Ha BY, Liu AJ. 1999. *Phys. Rev.* E60:803
150. Solis FJ, De la Cruz MO. 1999. *Phys. Rev.* E60:4496
151. Lyubartsev AP, Tang JX, Janmey PA, Nordenskiöld L. 1998. *Phys. Rev. Lett.* 81:5465
152. Ray J, Manning GS. 1994. *Langmuir* 10:2450
153. Schneider J, Hess W, Klein R. 1985. *J. Phys. A Gen. Phys.* 18:1221
154. Graf H, Lowen H. 1999. *Phys. Rev.* E59:1932
155. Stevens M. 1999. *Phys. Rev. Lett.* 82:101
156. Podgornik R, Parsegian VA. 1998. *Phys. Rev. Lett.* 80:1560
157. Van Olphen H. 1977. *Caly Colloid Chemistry.* New York: Wiley. 2nd ed.

158. Dubois M, Zemb T, Belloni L, Delville A, Levitz P, Setton R. 1992. *J. Chem. Phys.* 96:2278
159. Pellenq RJM, Caillol JM, Delville A. 1997. *J. Phys. Chem.* 101:8584
160. Delville A, Dajmeddine G, Pellenq RJM, Caillol JM, Van Damme H. 1998. *Langmuir* 14:5077
161. Boek ES, Coveney PV, Skipper NT. 1995. *J. Am. Chem. Soc.* 117:12608
162. Trizac E, Hansen JP. 1997. *Phys. Rev.* E56:3137
163. Leote de Carvalho RJF, Trizac E, Hansen JP. 2000. *Phys. Rev. E* 61:1634
164. Delville A. 1999. *J. Phys. Chem.* B103:8296
165. Hansen JP, Trizac E. 1997. *Physica A* 235:257
166. Leote de Carvalho RJF, Trizac E, Hansen JP. 1998. *Europhys. Lett.* 43:369
167. Mourchid A, Delville A, Lambard J, Lécolier E, Levitz P. 1995. *Langmuir* 11:1942
168. Pignon F, Magnin A, Piau JM, Cabane B, Lindner P, Diat O. 1997. *Phys. Rev.* E56:3281
169. Kroon M, Vos WL, Wegdam GH. 1998. *Phys. Rev.* E57:1962
170. Bonn D, Kellay H, Tanaka H, Wegdam GH, Meunier J. 1999. *Langmuir* 15: 7534
171. Kutter S, Hansen JP, Sprik M, Boek E. 2000. *J. Chem. Phys.* 112:311
172. Rowan D, Hansen JP, Trizac E. Submitted for publication
173. Dijkstra M, Hansen JP, Madden PA. 1997. *Phys. Rev.* E55:3044
174. Pincus PA, Safran SA. 1999. *Europhys. Lett.* 42:103
175. Levesque D, Weis JJ, Patey GN. 1980. *J. Chem. Phys.* 72:1887
176. Carnie SL, Chan YC, Walker GR. 1981. *Mol. Phys.* 43:1115
177. Kusalik PG, Patey GN. 1988. *J. Chem. Phys.* 88:7715
178. Blum L, Vericat F, Degreve L. 1999. *Physica A* 256:396
179. Berendsen HJC, Grigera JR, Straatsma TP. 1987. *J. Phys. Chem.* 91:6269
180. Kralj-Iglič V, Iglič A. 1996. *J. Phys. Paris* 6:477
181. Borukhov I, Andelman D, Orland H. 1997. *Phys. Rev. Lett.* 79:435
182. Tang Z, Scriven LE, Davis HT. 1994. *J. Chem. Phys.* 100:4527
183. Otto F, Patey GN. 1999. *Phys. Rev.* E60:4416
184. Frink LJD, van Swol E. 1996. *J. Chem. Phys.* 105:2884
185. Carnie SL, Chan DYC. 1980. *J. Chem. Phys.* 73:2949
186. Blum L, Henderson D. 1981. *J. Chem. Phys.* 74:1902
187. Diaz-Herrera E, Forstmann F. 1995. *J. Chem. Phys.* 102:9005
188. Rosenfeld Y. 1993. *J. Chem. Phys.* 98:8126
189. Rosenfeld Y, Schmidt M, Löwen H, Tarazona P. 1997. *Phys. Rev.* E55: 4245
190. Biben T, Hansen JP, Rosenfeld Y. 1998. *Phys. Rev.* E57:R3727
191. Augousti AT, Rickayzen G. 1984. *J. Chem. Soc. Faraday Trans.* 80:141
192. Kinoshita M, Iba S, Harada M. 1996. *J. Chem. Phys.* 105:2487
193. Tandon S, Kesavamoorthy R, Asher SA. 1998. *J. Chem. Phys.* 109:6490
194. Netz RR, Orland H. 1999. *Europhys. Lett.* 45:726
195. Henderson D, ed. 1991. *Fundamentals of Inhomogenous Fluids*. New York: Dekker
196. Deutsch C, Gombert MM, eds. 2000. *Strongly Coupled Coulomb Systems*. Orsay, FR: EDP Sci.

Annual Review of Physical Chemistry
Volume 51, 2000

CONTENTS